Comput Mech (2006) 38: 51–60
DOI 10.1007/s00466-005-0720-3

ORIGINAL PAPER

H. Wang · Q-H. Qin · Y-L. Kang

A meshless model for transient heat conduction in functionally graded materials

Received: 20 December 2004 / Revised: 17 May 2005 / Published online: 31 August 2005

Abstract A meshless numerical model is developed for analyzing transient heat conduction in non-homogeneous functionally graded materials (FGM), which has a continuously functionally graded thermal conductivity parameter. First, the analog equation method is used to transform the original non-homogeneous problem into an equivalent homogeneous one at any given time so that a simpler fundamental solution can be employed to take the place of the one related to the original problem. Next, the approximate particular and homogeneous solutions are constructed using radial basis functions and virtual boundary collocation method, respectively. Finally, by enforcing satisfaction of the governing equation and boundary conditions at collocation points of the original problem, in which the time domain is discretized using the finite difference method, a linear algebraic system is obtained from which the unknown fictitious sources and interpolation coefficients can be determined. Further, the temperature at any point can be easily computed using the results of fictitious sources and interpolation coefficients. The accuracy of the proposed method is assessed through two numerical examples.

Keywords Transient heat conduction · Virtual boundary collocation method · Fundamental solution · Superposition principle · Radial basis functions · Analog equation method · Functionally graded media.

H. Wang · Y.-L. Kang
Department of Mechanics, Tianjin University,
Tianjin, 300072 P.R. China

Q.-H. Qin (✉)
Department of Engineering, Australian National University,
Canberra, ACT 0200, Australia
E-mail: qinghua@qin@anu.edu.au

1 Introduction

Due to its excellent thermal properties, transient heat conduction problems in FGMs exist in many engineering processes, such as electronic cooling, encapsulation and cryogenics, and have received a considerable attention from researchers. However, because of the intrinsic complexity of the corresponding governing equation, analytical solutions are usually difficult to obtain except for problems with simple geometry and boundary conditions. As a result, various numerical models have been developed for analyzing transient heat conduction problems [1, 2].

It is noted that numerical methods such as the finite element method (FEM), finite difference method (FDM) and boundary element method (BEM) have been well established over the past few decades and have been successfully applied to transient heat conduction problems [1, 2]. Compared to FEM and FDM, BEM generally involves boundary discretization only and the governing differential equation is satisfied exactly inside the domain. This is an important advantage over domain-type methods such as FEM and FDM. However, the use of BEM, based on discretization in time, usually results in domain integrals which may increase computing time and even cause some numerical problems [1]. In particular, a time-consuming domain integral is required when calculating temperatures at internal points, which makes BEM relatively inefficient compared to FEM and FDM. To overcome the inefficiency, several approaches based on conventional boundary integral equations have been developed to compute domain integrals engendered by time and inhomogeneous terms. A frequently used method is the dual reciprocity boundary element method (DRBEM) [3], which converts the domain integral occurring in BEM equations into a boundary integral by using a set of locally based radial functions (RBF) to approximate the inhomogeneous term related to the particular solution. The application of this approach to the tran-

sient heat conduction problem can be found in [4–7]. The multiple reciprocity boundary element method (MRBEM) appeared in [8] is also an efficient method for dealing with domain integrals. It removes the domain integral in a recurrent manner by introducing higher order fundamental solutions.

Alternatively, meshless methods have received considerable attention in recent years because of their lack of dependence on mesh and avoiding meshing, remeshing, mesh distortion in large deformation cases and easy to prepare initial data. At present, meshless methods can be divided into two major categories: domain-based and boundary-based. Compared to domain-based meshless methods, boundary-based meshless methods inherit the advantages of BEM and mainly collocate points on the boundary or sub-boundary. Since the method developed in this paper can be viewed as a boundary-based meshless method, developments corresponding to this category only are briefly reviewed here. Zhu et al. [9] developed a local boundary integral equation (LBIE) method by dividing the entire domain into several small subdomains, in which LBIE and moving least square (MLS) approximation are used. Sladek et al. [10] applied this method to analyze transient heat conduction problem in FGM. Recently, Chen [11, 12] derived a boundary particle method (BPM) based on the multiple reciprocity principle and the nonsingular higher-order general solution and applied it to convection-diffusion problems. In addition to the above direct boundary-based meshless methods, there are indirect ones. The method of fundamental solution (MFS) [13] is an indirect method involving no mesh or integration which has advantages of simplicity and effectiveness. This method essentially uses fictitious source points outside the solution domain and the corresponding fundamental solutions to approximate the target function. The unknown coefficients of the fundamental solutions and the coordinates of the fictitious sources are found by forcing the approximation to satisfy the boundary conditions. There are other similar methods such as the virtual boundary collocation method (VBCM) [14] and charge simulation method [15], in which the locations of fictitious source points are fixed and the only unknowns are the coefficients of the fundamental solutions. However, the methods mentioned above have not included a process for dealing with body sources. The combination of MFS and RBF provides the possibility of developing a real meshless method. From the early version of RBF, $1+r$, to compactly support RBFs (CS-RBF), the rich class of RBFs has been widely used due to the improvement in accuracy and solid mathematical foundation. The most popular RBFs are polyharmonic splines, thin plate spline (TPS) and multiquadrics (MQs), which are all globally supported, and have been applied successfully to many engineering problems. However, as suggested in ref. [16, 17], the user must be very careful about the order of the basis function. It should be as low as the application tolerance, and any excessive order will have negative effects on stability. Furthermore, for low density interpolation points, a high-order basis function can be used, and for higher density interpolation points, a low-order basis function should be employed to avoid numerical problems. Additionally, augmented polynomials can increase stability and accuracy.

In this paper, a (VBCM) [14] in conjunction with RBF approximation and the analog equation method (AEM) [18] is developed to analyze transient heat conduction problems in FGM. AEM is introduced to convert the original governing differential equation to an equivalent Poisson's equation, which has a simpler fundamental solution than the fundamental solution of the original problem required in most boundary-type methods. RBF approximation is then employed to derive the particular solutions related to the fictitious internal source which appears when AEM is introduced and VBCM is used to implement the corresponding homogeneous solutions. Further, the full solution at a particular time is constructed by adding the two parts mentioned above. In the derivation, the time domain is discretized using the finite difference method. Enforcing satisfaction of the boundary conditions and governing equation at certain collocation points yields a linear algebraic system, from which unknown sources and interpolation coefficients at any particular time can be determined. Further, the field function at random points can be computed at a particular time.

2 Basic formulas of transient heat conduction

Consider a transient heat conduction problem, occupying an arbitrarily shaped region Ω bounded by its boundary Γ. In the Cartesian coordinates system, the transient temperature field in a FGM or a heterogeneous isotropic medium is governed by the diffusion equation

$$\nabla \cdot (k\nabla u) + f(X,t) = k\nabla^2 u + \nabla k \cdot \nabla u + f(X,t) = \rho c \frac{\partial u(X,t)}{\partial t} \tag{1}$$

with the boundary conditions:

–Dirichlet boundary condition related to unknown temperature field is

$$u(X,t) = \bar{u}(X,t) \quad X \in \Gamma_1 \tag{2a}$$

–Neumann boundary condition for the boundary heat flux is

$$q(X,t) = \bar{q}(X,t) \quad X \in \Gamma_2 \tag{2b}$$

–Convection or Robin boundary condition is

$$q(X,t) = h_\infty(u - u_\infty) \text{ or } h_\infty u - q = h_\infty u_\infty \quad X \in \Gamma_3 \tag{2c}$$

where ∇^2 represents the Laplacian operator, t denotes time ($t > 0$). k is the thermal conductivity dependent on the special variables $X \in \Omega \subset R^d$, d is the dimension of the domain is Ω; ρ is the mass density and c is the specific heat. $f(X,t)$ stands for the internal heat source

generated per unit volume. q represents the boundary heat flux defined by $q = -k\nabla u \cdot \mathbf{n} = -k\frac{\partial u}{\partial n}$, n is the unit outward normal to the boundary Γ. $\bar{u}$ and $\bar{q}$ are specified values on the boundary. The constant h_∞ is the convection coefficient and u_∞ is the environmental temperature. For a well-posed problem, we have $\Gamma = \Gamma_1 \cap \Gamma_2 \cap \Gamma_3$.

For functionally graded materials (FGM), for instance, assume that the thermal conductivity varies exponentially in one Cartesian coordinate, i.e.,

$$k(x) = k_0 e^{\lambda x}, \tag{3}$$

where λ is the non-homogeneity parameter. Specially, for homogeneous and isotropic materials, the thermal conductivity k is a constant. In this case, Eq. (1) can be simplified as a popular hyperbolic poisson equation,

$$k\nabla^2 u + f(X,t) = \rho c\frac{\partial u}{\partial t}, \tag{4}$$

which has been studied by many researchers.

Finally, the initial condition must be supplied

$$u(X, t=0) = g(X). \tag{5}$$

3 Numerical process

A meshless model for solving the hyperbolic boundary value problem (BVP) defined by Eqs. (1), (2a)–(2c) and (5) is derived in this section. We start by converting Eq. (1) into a simple Poisson equation using the analog equation method. We then consider the RBF approximation of the fictitious loading term induced in the converting process. Finally a virtual boundary collocation formulation is given for two-dimensional problems.

3.1 The analog equation method (AEM) [18]

Suppose $u'(X) = u(X,t)$ is the solution sought at a particular time t to the boundary value problem (BVP) defined by Eqs. (1), (2a)–(2c) and (5). Assume also $u(X,t)$ to be two times continuously differentiable in Ω. Applying the analog equation method to Eq. (1), we have

$$\nabla^2 u^t = b^t(X) \tag{6}$$

together with the boundary conditions as described in Eqs. (2a)–(2c) and the initial condition as given in Eq. (5). The fictitious source $b^t(X)$, here, may be evaluated in many ways, including global RBF approximation and CS-RBF approximation. The simplest and most efficient way to evaluate $b^t(X)$ is the global RBF function approach discussed in Sect. 3.2. In addition, to make the derivation tractable, we can decompose u^t at any particular time t into two major parts: the homogeneous solution u_h^t and the inhomogeneous solution or particular solution u_p^t

$$u^t = u_h^t + u_p^t \tag{7}$$

where u_h^t and u_p^t satisfy respectively

$$\nabla^2 u_p^t(X) = b^t(X) \tag{8}$$

and

$$\begin{cases} \nabla^2 u_h^t(X) = 0 & X \in \Omega \\ u_h^t(X) = \bar{u}^t - u_p^t(X) & X \in \Gamma 1 \\ q_h^t(X) = \bar{q}^t - q_p^t(X) & X \in \Gamma 2 \\ h_\infty u_h^t(X) - q_h^t(X) = h_\infty u_\infty - h_\infty u_p^t + q_p^t & X \in \Gamma 3 \end{cases} \tag{9}$$

3.2 The RBF approximation for the particular solution u_p^t

In this section a RBF approximation is presented for evaluating the particular solution at any given time t. The right-hand term of Eq. (8) can be approximated by [3–7]

$$b^t(X) = \sum_{j=1}^{M} a_j^t f_j(X) \tag{10}$$

where M is the number of interpolation points including interior and boundary points as shown in Fig. 1; α_j^t are coefficients to be determined, and f_j are a set of RBF.

Similarly, the particular solution u_p^t and its normal derivative are also approximated in the form

$$u_p^t(X) = \sum_{j=1}^{M} \alpha_j^t \hat{u}_j(X) \tag{12}$$

$$q_p^t(X) = -k\left[\sum_{j=1}^{M} \alpha_j^t \frac{\partial \hat{u}_j}{\partial n}\right] \tag{13}$$

where $\hat{u}_j$ and $\hat{q}_j$ are a corresponding set of particular solutions and its normal derivatives, respectively. Because the particular solution u_p^t satisfies Eq. (8), the key to this approximation is the existence of a corresponding set of approximating particular solutions $\hat{u}_j$, which are largely dependent on the underlying differential operator

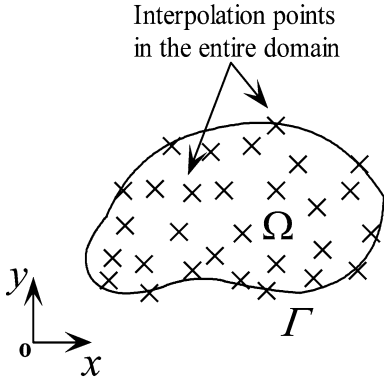

Fig. 1 Distribution of interpolation points within the physical domain and on its boundary

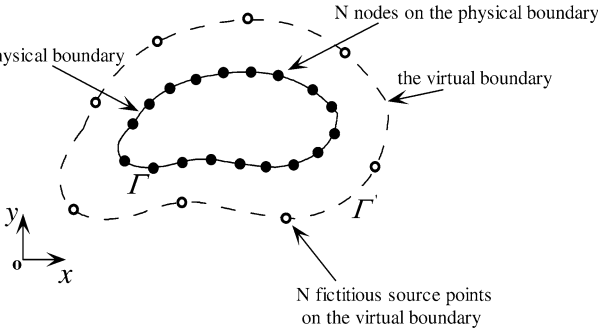

Fig. 2 Illustration of the computational domain and collocation points discretization on the physical and virtual boundaries

and the choice of RBF f_j. Noting that, in Eq. (8), only the Laplacian operator is involved, a set of particular solutions $\hat{u}_j$ can be chosen in such a way that

$$\nabla^2 \hat{u}_j(X) = f_j(X) \quad (j = 1 \to M) \tag{14}$$

The effectiveness and accuracy of the interpolation depends on the choice of the RBFs f_j. Besides the ad-hoc function $1+r$ [19], which is merely a special type of RBF [20] that is used almost exclusively and uncritically in the engineering literature, the three radial basis functions, polyharmonic splines, TPS and multiquadrics (MQ) are also commonly used in meshless formulation. $r(X, X_j) = r_j(X) = |X - X_j|$ here denotes the distance from the source point X_j to the field point X. In this paper, different orders of RBFs f_j are investigated in Sect. 4 to demonstrate their accuracy and stability for time-dependent heat conduction problems.

Since the inhomogeneous term $b^t(X)$ is an unknown function depending on the unknown function $u^t(X)$, the coefficients α_j^t cannot be determined directly through solving Eq. (10). However, this problem can be tackled in the way described below.

3.3 Virtual boundary collocation method (VBCM) for the homogeneous solution

To obtain a weak solution of Laplace problem (9), N collocation points $X_j\,(j = 1, 2, \ldots, N)$ on the physical boundary and N fictitious source points $X_i'\,(i = 1, 2, \ldots, N)$ on the virtual boundary are selected. Moreover, it is assumed that at each source point there exists a virtual load $\varphi_i (1 \le i \le N)$. The potential u_h^t and the boundary heat flux at field points X in the domain or on the boundary can be expressed by a linear combination of fundamental solutions in terms of fictitious sources located on the virtual boundary [13, 14], that is

$$u_h^t(X) = \sum_{i=1}^{N} \varphi_i^t u^*(X, X_i') \tag{15}$$

$$q_h^t(X) = -k\left[\sum_{i=1}^{N} \varphi_t^i \frac{\partial u^*}{\partial n}\right] \tag{16}$$

in which u^* and q^* are the fundamental solution of the Laplacian operator and its normal derivative,

$$u^*(X, X') = \frac{1}{2\pi} \ln \frac{1}{r(X, X')} \tag{17}$$

$$\begin{aligned} q^*(X, X') &= \frac{\partial u^*(X, X')}{\partial n} = \frac{\partial u^*(X, X')}{\partial r} \frac{\partial r}{\partial n} \\ &= -\frac{1}{2\pi r} \cos(r, n) \end{aligned} \tag{18}$$

for 2-D problems.

It should be mentioned that a boundary with a shape similar to that of the physical boundary, or simply a circular boundary for the 2D domain and a spherical boundary for 3D problems, are usually selected as the shape of the virtual boundary. A virtual boundary which mimicked the shape of the physical boundary was used by Sun et al. [14] because of the advantage of maintaining the source at roughly the same magnitude from the physical boundary. However, the construction of a similar virtual boundary may be inconvenient, especially for complicated boundaries. A circular virtual boundary has good flexibility and can be applied easily to most problems. But in some cases, differences of large magnitude may be encountered which lead to ill-conditioned solutions.

The distance between the fictitious source point and the physical boundary is another interesting issue in the present meshless model. Theoretically, there are no rules for selecting the location of the virtual boundary. However, from the point of view of computation and considering the singularity of the fundamental solution, the accuracy of the result will degrade when the distance between the virtual and physical boundaries becomes very close [14]. Conversely, round-off error in C/Fortran floating point arithmetic may be a serious problem when the source points are far from the physical boundary. In that case, the coefficient matrix of the system of equations is nearly zero [19, 20]. For a virtual boundary that is similar in shape to the physical boundary, the location can be determined by defining the similarity ratio between the virtual and physical boundaries as

$$\text{similarity ratio} = \frac{\text{characteristic length of the virtual boundary}}{\text{characteristic length of the physical boundary}}$$

For a circular virtual boundary, the center of the circle may overlap with the center of the domain, and the radius is an important parameter to measure its location. In particular, for a rectangular domain, the real parameter β (Fig. 3), representing the similarity ratio of the similar virtual boundary, can measure the radius of the circular virtual boundary.

The shape and location of the virtual boundary are discussed in Sec. 4.

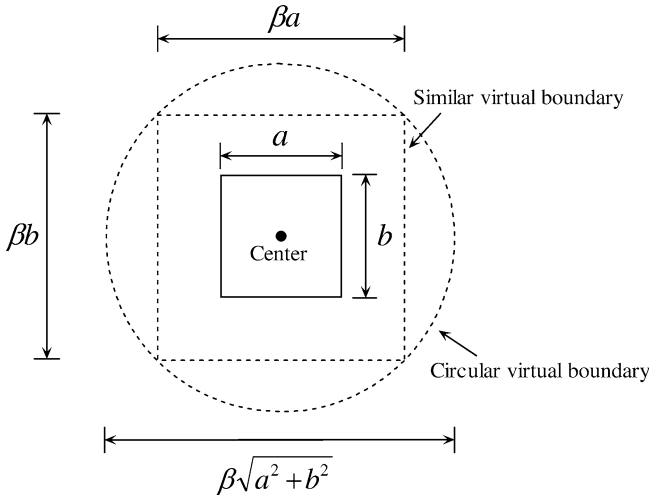

Fig. 3 Similar and circular virtual boundaries for a rectangular domain

3.4 The backward time stepping scheme

Based on the discussion above, the solution $u^t(X)$ to Eqs. (1) and (2a)–(2c) at a particular time t can be written as

$$u^t(X) = \sum_{i=1}^{N} \varphi_i^t u^*(X, X_i') + \sum_{j=1}^{M} \alpha_j^t \hat{u}_j(X) \tag{19}$$

$$q^t(X) = -k\left(\sum_{i=1}^{N} \varphi_i^t \frac{\partial u^*}{\partial n} + \sum_{j=1}^{M} \alpha_j^t \frac{\partial \hat{u}_j}{\partial n}\right) \tag{20}$$

Differentiating Eq. (19) with respect to x or y yields

$$u^t_{,xx} = \sum_{i=1}^{N} \varphi_i^t u^*_{,xx} + \sum_{i=1}^{M} \alpha_j^t (\hat{u}_j)_{,xx}, \tag{21a}$$

$$u^t_{,yy} = \sum_{i=1}^{N} \varphi_i^t u^*_{,yy} + \sum_{i=1}^{M} \alpha_j^t (\hat{u}_j)_{,yy}, \tag{21b}$$

$$u^t_{,x} = \sum_{i=1}^{N} \varphi_i^t u^*_{,x} + \sum_{i=1}^{M} \alpha_j^t (\hat{u}_j)_{,x}, \tag{21c}$$

$$u^t_{,y} = \sum_{i=1}^{N} \varphi_i^t u^*_{,y} + \sum_{i=1}^{M} \alpha_j^t (\hat{u}_j)_{,y}. \tag{21d}$$

The formulations given in Sects 3.1, 3.2 and 3.3 are in terms of a particular time t. In order to obtain the temperature field and its flux at any time, the time domain is divided into elements and a simple backward time stepping scheme is used, i.e.,

$$\left.\frac{\partial t}{\partial t}\right|_{t+\Delta t} = \frac{u^{t+\Delta t} - u^t}{\Delta t}, \tag{22}$$

where Δt is the time step.

Substituting Eq. (22) into Eqs. (1) and (2a)–(2c), we have

$$\begin{aligned} &k\nabla^2 u^{t+\Delta t} + \nabla k \cdot \nabla u^{t+\Delta t} - \frac{\rho c}{\Delta t} u^{t+\Delta t} \\ &= -\frac{\rho c}{\Delta t} u^t(X) - f^{t+\Delta t}(X) \end{aligned} \tag{23}$$

with boundary conditions

$$u^{t+\Delta t}(X) = \bar{u}^{t+\Delta t} \quad \text{on } \Gamma_1 \tag{24a}$$

$$q^{t+\Delta t}(X) = \bar{q}^{t+\Delta t} \quad \text{on } \Gamma_2 \tag{24b}$$

$$q^{t+\Delta t}(X) = h_\infty(u^{t+\Delta t} - u_\infty) \quad \text{on } \Gamma_2 \tag{24c}$$

Using Eqs. (19), (20) and (21a)–(21d), satisfaction of the governing equation (23) at M interpolation points inside Ω and the boundary conditions (24a)–(24c) at N nodal points on the physical boundary provides $N + M$ equations to determine unknowns α_j^t and φ_i^t:

$$\begin{cases} \sum_{i=1}^{N} \varphi_i^{t+\Delta t}\left(k\nabla^2 u^* + \nabla k \cdot \nabla u^* - \frac{\rho c}{\Delta t} u^*\right) + \\ \quad \sum_{j=1}^{M} \alpha_j^{t+\Delta t}\left(k\nabla^2 \hat{u}_j + \nabla k \cdot \nabla \hat{u}_j - \frac{\rho c}{\Delta t}\hat{u}_j\right) \\ \quad = -f^{t+\Delta t} - \frac{\rho c}{\Delta t} u^t \\ \sum_{i=1}^{N} \varphi_i^{t+\Delta t} u^* + \sum_{j=1}^{M} \alpha_j^{t+\Delta t} \hat{u}_j = \bar{u}^{t+\Delta t} \\ \sum_{i=1}^{N} \varphi_i^{t+\Delta t}\left(-k\frac{\partial u^*}{\partial x_m} n_m\right) + \sum_{j=1}^{M} \alpha_j^{t+\Delta t}\left(-k\frac{\partial \hat{u}_j}{\partial x_m} n_m\right) = \bar{q}^{t+\Delta t} \\ \sum_{i=1}^{N} \varphi_i^{t+\Delta t}\left(h_\infty u^* + k\frac{\partial u^*}{\partial x_m} n_m\right) + \sum_{j=1}^{M} \alpha_j^{t+\Delta t}\left(h_\infty \hat{u}_j + k\frac{\partial \hat{u}_j}{\partial x_m} n_m\right) \\ \quad = h_\infty u_\infty \end{cases} \tag{25}$$

The unknown coefficients $\alpha_j^{t+\Delta t}$ and $\varphi_t^{t+\Delta t}$ can thus be determined by solving the linear algebraic system (25) and using the initial condition Eq. (5). Once these unknown coefficients are determined, the solution $u^{t+\Delta t}$ and it normal derivative at any field point X in the domain or on its boundary can be calculated using Eqs. (19) and (20).

Here, we notice that the process described above (Sects. 3.1 to 3.4) is fully independent on the original problem. Only the formation of equation (25) involves the original different equations. Therefore, the proposed meshless method has high adaptation to solve other potential problems, for example, nonlinear heat conduction problems in the case that the thermal conductivity is in terms of temperature field or the internal source $\boldsymbol{f}(\boldsymbol{X}, \boldsymbol{t})$ is function of temperature. The only difference is that Eq. (25) in this case is a nonlinear algebraic system and can be solved by means of iterative methods.

4 Numerical implementation

In order to demonstrate the efficiency and accuracy of the proposed meshless method and the selected RBF and virtual boundary, a transient heat conduction in isotropic materials is first considered since corresponding

exact results can be used for verification. Then the transient heat conduction in the functionally graded materials is discussed. Though the proposed meshless method has no restrictions on the spatial variation of the material parameters of FGM, the numerical example presented here is restricted to an exponential variation of the material properties with Cartesian coordinates for the purpose of comparison.

Example 1 Consider a benchmark problem [7] whose geometry is a unit square in which no internal heat source exists. Zero initial temperature has been assumed and homogeneous Neumann boundary conditions (insulation) are prescribed on the sides $x = 0$, $y = 0$ and $y = 1$, respectively. The remaining side is subjected to a sudden unit temperature jump. The geometry and boundary conditions of the problem are shown in Fig. 4.

Using the method of variable separation, the analytic solution can be obtained as

$$u(x,t) = 1 - \sum_{i=0}^{\infty} (-1)^i \frac{4}{(2i+1)\pi} \cos(\mu_i x) \exp(-\mu_i^2 t)$$

$$q(x,t) = -k \times \left(\sum_{i=0}^{\infty} (-1)^i \frac{4\mu_i}{(2i+1)\pi} \sin(\mu_i x) \exp(-\mu_i^2 t) \right) \times n_x$$

with μ_i defined by

$$\mu_i = (2i+1)\pi/2$$

In the computation, thermal diffusivity $a = 1\ \mathrm{m}^2/\mathrm{s}$ and thermal conductivity of materials $k = 1\ \mathrm{W/(m \cdot ^\circ C)}$ is assumed. The uniform interpolation scheme is used in the domain. A total of 20 fictitious source points are selected on the virtual boundary and 121 uniform interpolation points are used, unless there is a special statement.

Firstly, both the first- and third-order BRFs, $1+r$ and $1+r^3$, which have been widely used in the literature, are used in the calculation and the corresponding results are compared. The numerical results in Fig. 6 show that the use of higher-order RBF interpolation functions does not improve computing accuracy in transient problems. This phenomenon has also been observed in previous work [16]. Therefore, care must be taken in using higher-order RBFs since the linear system associated with the computation of the particular solution can easily result in an ill-conditioned number, which is directly linked to the order of the radial basis functions and density of the interpolation points. In contrast, low-order RBF functions can maintain the necessary accuracy and stability, especially for time-dependent problems, in which the dominant error is presumably caused by the time-stepping scheme [16, 17]. Therefore, the first-order interpolation function $1+r$, also known as the ad-hoc function, is employed first in the following computation.

In Fig. 6, the effects of different source distributions, rectangular and circular virtual boundary in this case, respectively, (see Fig. 5) are also considered. Assume that the similarity ratio is 3.0 and thus the corresponding radius of the circular virtual boundary is $3.0\times\sqrt{2}/2$ (see Fig. 3). The relative error of temperature at $t = 0.5$ s is

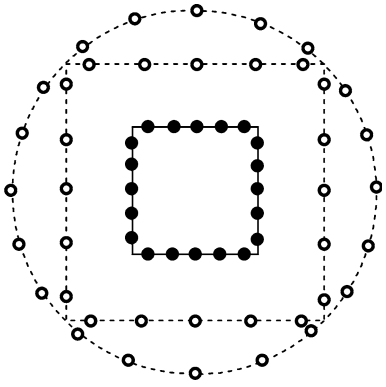

Fig. 5 Configuration of collocation points on the virtual and physical boundaries

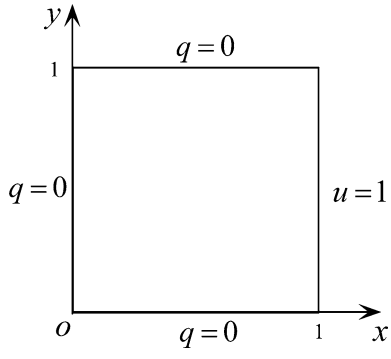

Fig. 4 Geometry of the benchmark problem and boundary conditions

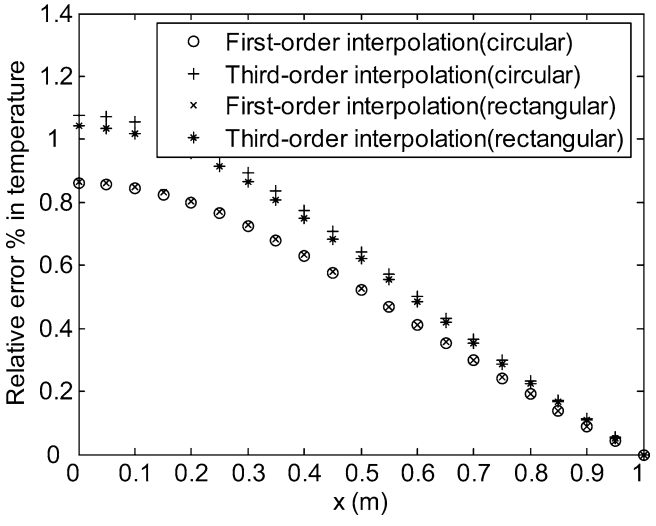

Fig. 6 Effect of order of RBF function on relative error of temperature at $t = 0.5$ s

computed along the line $y = 0.5$ m and with time steps of $\Delta t = 0.01$ s. It is evident from Fig. 6 that no distinct difference is observed; the results demonstrate that the use of both rectangular and circular virtual boundaries can yield acceptable results. The shape of virtual boundary has little influence on results when the similarity ratio is 3.0 or above. Therefore, a virtual boundary similar in shape to the physical one is used in the following computation unless a special statement is made.

To study the effect of the location of the virtual boundary on the accuracy of the proposed algorithm, Fig. 7 presents the relative error of temperature versus similarity ratio (defined in Sect 3.3) at point (0.5, 0.5) with time step $\Delta t = 0.01$ s. The results in Fig. 7 show that good computational accuracy and stability is achieved when the similarity ratio is greater than 2, and the optimal value of the similarity ratio is between 2.5–5.0. Although the virtual boundary can theoretically be chosen arbitrarily outside of the domain, either too small or too great a distance between the virtual and physical boundaries will reduce accuracy, due to the singularity of the fundamental solution and the restriction of computer precision including round-off error [14, 22].

Figure 8 shows the percentage error of temperature for two different time steps. It can be seen that the smaller the time step, the greater the accuracy of the results obtained. However, more computational time will inevitably be required if a smaller time step is chosen. Additionally, further reduction in the time step doesn't reduce the relative error [17].

Example 2 Consider a functionally graded finite strip with a unidirectional variation of thermal conductivity [10]. In this example, zero initial temperature is considered and the same exponential spatial variation for thermal conductivity and diffusivity is assumed

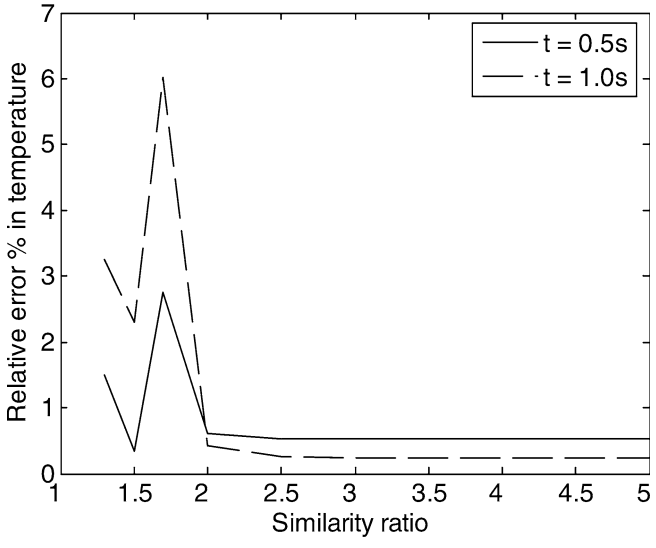

Fig. 7 Effect of similarity ratio on temperature at point (0.5, 0.5) with $\Delta t = 0.01$ s

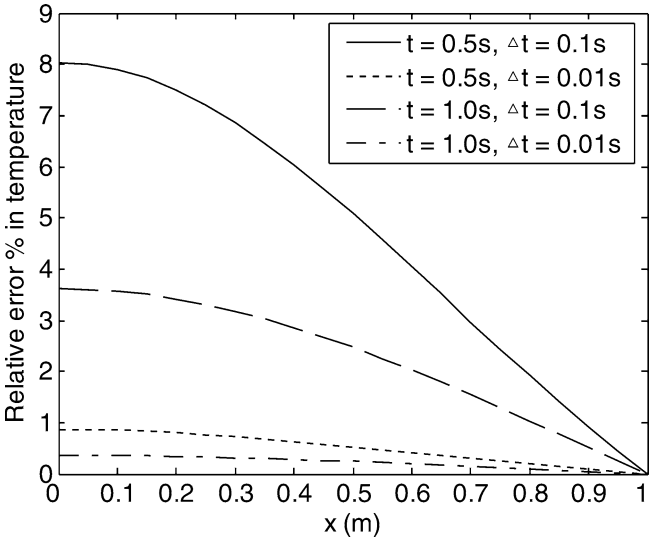

Fig. 8 Effect of time step on relative error of temperature (similarity ratio = 3.0)

$$k(X) = k_0 e^{\lambda x}$$

$$a = \frac{k}{\rho c} = a_0 e^{\lambda x}$$

where $k_0 = 17$ W/m°C and $a_0 = 0.17 \times \text{m}^2/\text{s}$. Two different exponential parameters $\lambda = 0.2$ and $0.5\ \text{cm}^{-1}$ [10] are assumed in numerical calculation. On the sides parallel to the y-axis two different temperatures are prescribed. One side is kept at zero temperature and the other has the Heaviside function of time, i.e., $u = T\,H(t)$ with $T = 1$°C. On the lateral sides of the strip the heat flux vanishes. In the numerical calculation, a square with side length $L = 0.04$ m is considered (see Fig. 9).

The special case with an exponential parameter $\lambda = 0$ is considered first. In this case the analytical solution is written as

$$u(x,t) = T\frac{x}{L} + \frac{2}{\pi}\sum_{n=1}^{\infty}\frac{T\cos n\pi}{n}\sin\frac{n\pi x}{L}\exp\left(-\frac{an^2\pi^2 t}{L^2}\right)$$

which can be used to check the accuracy of the present numerical method. Numerical results are obtained using

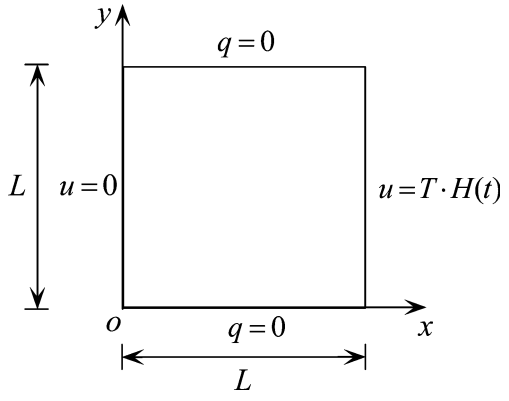

Fig. 9 Geometry of a functionally graded finite square strip and boundary conditions

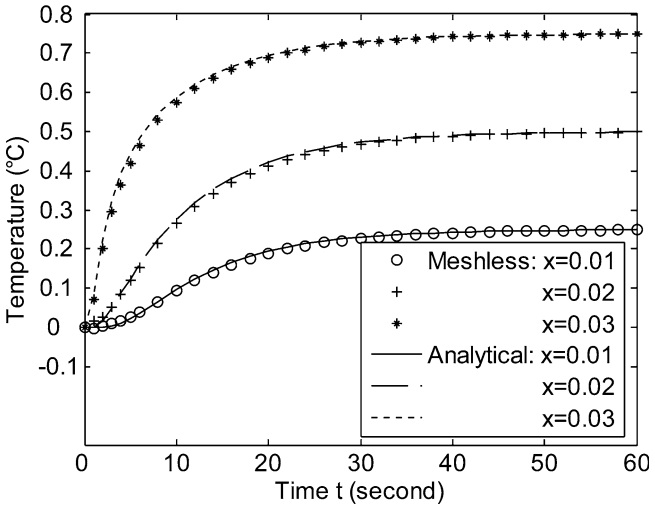

Fig. 10 Time variation of temperature in a finite square strip at three different positions with $\lambda = 0$

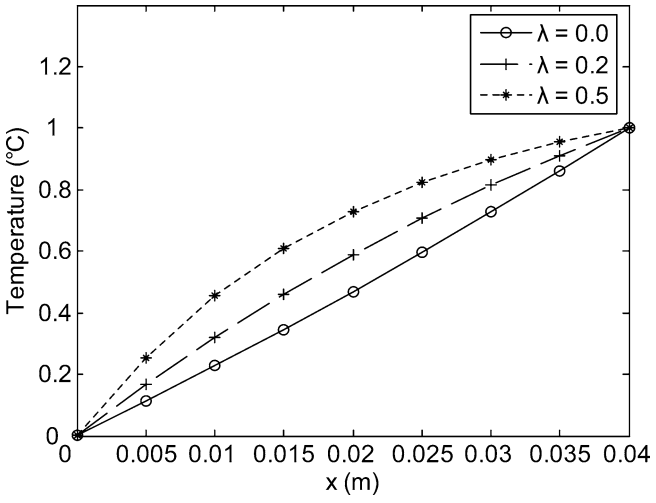

Fig. 12 Distribution of temperature at $t = 30$ s along x-axis of functionally graded finite square strip

36 fictitious source points, 169 interpolation points, similarity ratio = 3.0 and, time step $\Delta t = 1$ s. The following computation is carried out using the first-order interpolation function $1+r$ only. Figure 10 shows the temperature field at the three points ($x = 0.01$ m, 0.02 m and 0.03 m). A good agreement between numerical and analytical results is observed from Fig. 10.

The discussion above concerns heat conduction in homogeneous materials only since analytical solutions can be used for verification. To illustrate the application of the proposed algorithm to the FGM, consider now the FGM with $\lambda = 0.2$, and 0.5 cm^{-1}, respectively. The variation of temperature with time for three λ-values and at position $x = 0.02$ m is presented in Fig. 11. Fig. 12 shows the distribution of temperature along the x-axis at $t = 30$ s. As expected, it is found from Fig. 11 that the temperature increases along with an increase in λ-values (or equivalently in thermal conductivity), and the temperature approaches a steady state when $t > 20$ s. It is observed from Fig. 12 that the temperature increases along with an increase in λ-values again.

For final steady state an analytical solution can be obtained as

$$u(x) = T\frac{e^{\lambda x-1}}{e^{\lambda}a-1} \quad \left(u \to T\frac{x}{a} \text{ with } \lambda \to 0\right)$$

Analytical and numerical results computed at time $t = 70$ s corresponding to stationary or static loading conditions are presented in Fig. 13. The numerical results are in good agreement with the analytical results for the steady state case.

For comparison, the results at some particular points obtained by both the proposed method and the meshless local boundary integral equation method (LBIEM)[10] are listed in Table 1. It can be seen from Table 1 that the results from the proposed method is slightly larger than those obtained LBIEM and after $t = 50$ s a relatively

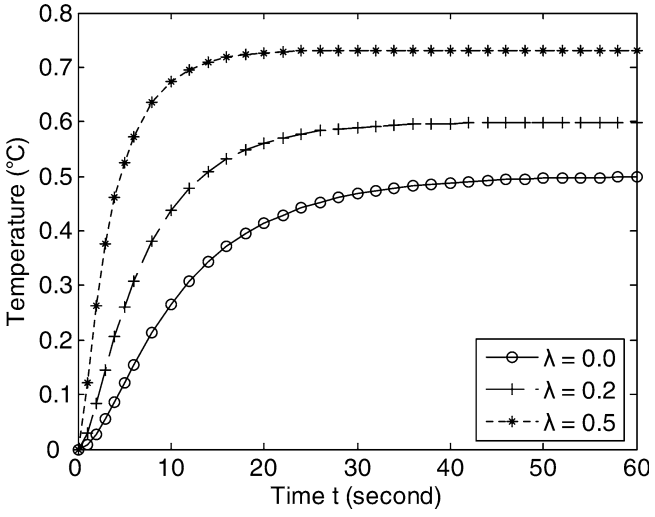

Fig. 11 Time variation of temperature at position $x = 0.02$ m of functionally graded finite square strip

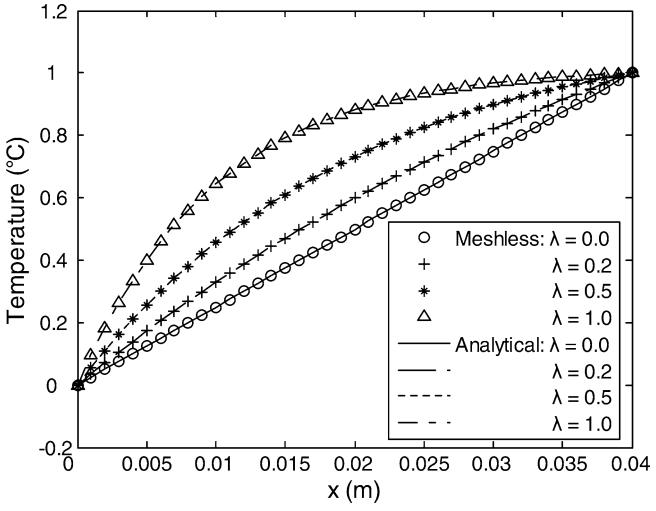

Fig. 13 Distribution of temperature along x-axis for a functionally graded finite square strip under steady-state loading conditions

Table 1 Comparison of LBIEM* and the proposed method at $\lambda = 0.5\text{cm}^{-1}$ and $x = 0.01$ m

	t = 10 s	t = 20 s	t = 30 s	t = 40 s	t = 50 s	t = 60 s	t = infinite
LBIEM	0.1871	0.3281	0.3800	0.3986	0.4019	0.4053	0.4581
Proposed method	0.3915	0.4497	0.4546	0.4550	0.4551	0.4551	0.4551
Exact	/	/	/	/	/	/	0.4551

(*the LBIEM results were obtained from Figs. 4 and 5 in reference [10])

steady state reaches. It should be here mentioned that the numerical solutions displyed from Figs. 4 and 5 in reference [10] probably have certain error to practical computing results produced by use of LBIEM. Moreover, the different treatment of time domain may also be the main reason causing the discrepancy. In the derivation of LBIEM [10], we noticed that Laplace transformation technology is used instead of the time stepping scheme. However, to the steady-state temperature field at $x = 0.01$ m, the two methods provided almost same results (see Table 1).

5 Conclusion

A meshless model is developed for analyzing transient heat conduction in FGMs. It is accomplished by an ingenious combination of VBCM with the analog equation method and RBF approximation. Although we note that the proposed method still has some disadvantages, such as the linear system of equations formed at length being dense and possibly being ill-conditioned for large and complex domains (which are also the common disadvantages of MFS and RBF approximation), the proposed meshless method has the following advantages compared with general boundary-based methods:

(1) the fundamental solutions used in general BEM

$$L^*(u^*) = \delta(x - \xi),$$

where $L^*(\cdot)$ is the adjoint operator to $L(\cdot)$ and $\delta(x - \xi)$ is the Dirac delta function, are usually complex and difficult to obtain. In contrast, the proposed meshless method requires the fundamental tsolution of the standard Laplacian operator only, even in complex problems.

(2) No boundary element is required in the method, and thus the general singular integral is avoided and the proposed method is fully independent of mesh.

(3) There are no extra equations required to compute the internal fields.

(4) Compared with other meshless methods, the computing process is relatively simple and efficient.

(5) No inversion of coefficient matrix is involved in the process of RBF approximation.

(6) There have no restrictions on exponential variation of the material properties with Cartesian coordinates. Therefore, other spatial variations of the material parameters of FGM can also apply.

(7) The proposed meshless method is easy to extend to nonlinear problems.

References

1. Ingber MS (1994) A triple reciprocity boundary element method for transient heat conduction analysis. In Boundary Element Technology, Brebbia CA, Kassab AJ (eds), vol. IX. Elsevier Applied Science Amsterdam, 41–49
2. Jirousek J, Qin QH (1996) Application of Hybrid-Trefftz element approach to transient heat conduction analysis, Compu Struc 58:195–201
3. Nardini D, Brebbia CA (1982) A new approach to free vibration analysis using boundary elements. In Boundary Element Methods in Engineering Proceedings. 4th International Seminar, Southampton. ed. C. A. Brebbia, Springer-Verlag, Berlin and New York, 312–326
4. Bulgakov V, Sarler B, Kuhn G (1998) Interative solution of systems of equations in the dual reciprocity boundary element method for the diffusion equation. Int J Numer Meth Eng 43:713–732
5. Blobner J, Bialecki RA, Kuhn G (1999) Transient non-linear heat conduction-radiation problems-a dual reciprocity formulation. Int J Numer Meth Eng 49:1865–1882
6. Singh KM, Tanaka M (1999) Dual reciprocity boundary element analysis of nonlinear diffusion-temporal discretization. Eng Anal Bound Elem 23:419–433
7. Bialecki RA, Jurgas P, Kuhn G (2002) Dual reciprocity BEM without matrix inversion for transient heat conduction. Eng Anal Bound Elem 26:227–236
8. Nowak AJ, Brebbia CA (1989) The multiple-reciprocity method. A new approach for transforming BEM domain integrals to the boundary. Eng Anal Bound Elem 6:164–167
9. Zhu T, Zhang JD, Atluri SN (1998) A local boundary integral equations (LBIE) method in computational mechanics, and a meshless discretization approach. Comput Mech 21:223–235
10. Sladek J, Sladek V, Zhang Ch (2003) Transient heat conduction analysis in functionally graded materials by the meshless local boundary integral equation method. Comput Mater Sci 28:494–504
11. Chen W (2002) High-order fundamental and general solutions of convection-diffusion equation and their applications with boundary particle method. Eng Anal Bound Elem 26:571–575
12. Chen W (2002) Meshfree boundary particle method applied to Helmholtz problems. Eng Anal Bound Elem 26:577–581
13. Kupradze VD (1965) Potential methods in the theory of elasticity. Israel Program for Scientific Translations. Jerusalem
14. Sun HC, Zhang LZ, Xu Q, Zhang YM (1999) Nonsingularity Boundary Element Methods, Dalian: Dalian University of Technology Press (in Chinese)
15. Golberg MA, Chen CS (1996) Discrete Projection Methods for Integral Equations. Computational Mechanics. Southampton

16. Ingber MS, Chen CS, Tanski JA (2004) A mesh free approach using radial basis functions and parallel domain decomposition for solving three-dimensional diffusion equations. Int J Numer Meth Eng 60:2183–2201
17. Schaback R (1995) Error estimates and condition numbers for radial basis function interpolation. Adv Comput Math 3:251–264
18. Katsikadelis JT (1994) The analog equation method - a powerful BEM - based solution technique for solving linear and nonlinear engineering problems. In: Brebbia CA, (ed) Boundary Element Method XVI, CLM Publications Southampton, p 167
19. Golberg MA, Chen CS (1999) The method of fundamental solutions for potential, Helmholtz and diffusion problems. Boundary Integral Methods: Numerical and Mathematical Aspects, In: Golberg MA(ed) Computational Mechanics Publications Southampton, 103–176
20. Mitic P, Rashed YF (2004) Convergence and stability of the method of meshless fundamental solutions using an array of randomly distributed sources. Eng Anal Bound Elem 28:143–153